Наносистеми, наноматеріали, нанотехнології
Nanosistemi, Nanomateriali, Nanotehnologii
2022, т. 20, № 2, сс. 305–320

PACS numbers: 32.30.Rj, 68.55.jd, 73.20.At, 73.61.Le, 78.70.En, 81.15.Cd, 82.80.Pv

XPS Investigation of Indium-Saving Indium–Tin Oxide (ITO) Thin Films

S. Petrovska[1], B. Ilkiv[1], O. Khyzhun[1], M. Ohtsuka[2], R. Sergiienko[3], L. Voisin[4], and T. Nakamura[2]

[1]*Frantsevych Institute for Problems of Materials Science, N.A.S. of Ukraine, 3, Krzhizhanovsky Str., UA-03142 Kyiv, Ukraine*
[2]*Institute of Multidisciplinary Research for Advanced Materials (IMRAM), Tohoku University, 980-8577 Sendai, Japan*
[3]*Physico-Technological Institute of Metals and Alloys, N.A.S. of Ukraine, 34/1, Academician Vernadsky Blvd., UA-03142 Kyiv, Ukraine*
[4]*Advanced Mining Technology Center (AMTC) and DIMin, Mining Engineering Department, University of Chile, Chile*

Indium–tin oxide (ITO) thin films with reduced to 50 mass.% indium oxide content are grown by direct current (DC) sputtering of ITO target in mixed argon–oxygen atmosphere onto glass substrates preheated at 523 K. The films showing the best electrical properties are subsequently heat-treated in air at temperatures of 523 and 623 K for 60 min. X-ray photoelectron spectroscopy (XPS) and x-ray emission spectroscopy (XES) are used for samples' characterization. Effects of oxygen-flow rate, Sn content, and heat-treatment temperature on electronic properties are studied and discussed. XPS measurements show that indium is in In^{3+} charge state, and tin is only in Sn^{4+} state in indium-saving ITO thin films sputtered at different conditions and heat-treated at different temperatures. As-deposited indium-saving ITO thin film sputtered at 0.5 cm^3_{STP}/min oxygen-flow rate, which demonstrates the highest conductivity among the as-deposited thin films, shows the highest relative intensity of O_{II} peak. The electron density of states increases when going from indium-saving thin film to typical ITO one.

Тонкі плівки оксиду Індію–Стануму (ІТО) з пониженим до 50% мас. вмістом оксиду Індію вирощували шляхом розпорошення мішені ІТО постійним струмом (DC) у змішаній атмосфері арґону та кисню на скляні підкладинки, попередньо нагріті до 523 К. Плівки, що демон-

стрували найкращі електричні характеристики згодом термічно обробляли на повітрі за температур у 523 та 623 К протягом 60 хв. Для характеризації зразків використовували рентґенівську фотоелектронну спектроскопію (РФС) і рентґенівську емісійну спектроскопію (РЕС). Вивчено й обговорено вплив витрати кисню, вмісту Sn та температури термооброблення на електронні властивості. Міряння за допомогою РФС показали, що Індій знаходиться в зарядовому стані In^{3+}, а Станум — лише в стані Sn^{4+} в тонких плівках ITO, розпорошених за різних умов і термічно оброблених за різних температур. Тонка плівка ITO з пониженим вмістом Індію, що розпорошувалася за швидкости потоку кисню у 0,5 $см^3$/хв. і продемонструвала найвищу провідність серед свіжонанесених тонких плівок, показала найвищу відносну інтенсивність піку $O_П$. Густина електронних станів зростала, коли переходили від плівки з пониженим вмістом Індію до типової тонкої плівки ITO.

Key words: indium–tin oxide, x-ray photoelectron spectroscopy, x-ray emission spectroscopy, thin films.

Ключові слова: оксид Індію–Стануму, рентґенівська фотоелектронна спектроскопія, рентґенівська емісійна спектроскопія, тонкі плівки.

(Received 5 July, 2021)

1. INTRODUCTION

Indium–tin oxide (ITO) thin films are still have been extensively investigated, since they can be used as semi-conducting window electrodes for solar cells, transparent conducting electrodes for liquid crystal displays (LCD), for optical solar reflectors [1–4]. However, increasing demand for ITO thin films for industry provoked high price of indium. Therefore, indium-saving films, which consist of a smaller quantity of In_2O_3 in its composition, were developed, and their properties were investigated [5–12]. It is well known that properties of materials are determined mainly by their electronic structure. Therefore, it is very important to study the electronic structure of the indium-saving ITO thin films. The electronic structure of conventional ITO thin films (90 mass.% In_2O_3) was studied in a great number of works [13–17], whereas it is known just several papers devoted to investigation of the electronic structure of indium-saving ITO thin films [18–20]. O'Neil *et al.* [18] found that the valence-band spectrum of $In_4Sn_3O_{12}$ can be resolved into three features, which are assigned to O2*p* states hybridized with In/Sn *d*, *p* and *s* states in order of increasing binding energy. According to calculations by projector-augmented-wave method [19], the valence bands just below the Fermi level are due O2*p* states with some In5*d* admixture.

A novelty of our work is to investigate the effect of heat-

treatment temperature together with effects of Sn content and oxygen flow rate in a wide range of values on the electronic structure of indium-saving ITO thin films.

In this investigation, ITO50 thin films with reduced to 50 mass.% amount of indium oxide sputtered onto glass substrates preheated at 523 K (PHS) were studied by x-ray photoelectron and x-ray emission spectra.

2. EXPERIMENTAL DETAILS

2.1. Sample Preparation

ITO50 (PHS) thin films were deposited onto glass substrates (Corning EAGLE 2000, surface of 50 mm×50 mm, thickness of 0.7 mm) preheated at 523 K by DC sputtering method using a ceramic ITO50 target (Mitsui Mining & Smelting, 50 mass.% In_2O_3–50 mass.% SnO_2). A schematic diagram of the sputtering apparatus (ULVAC, CS-200) used in the present study is shown in previously published article [5].

DC power source was used to sputter the ITO50 target. Process chamber was vacuumed at 10^{-5} Pa for its base pressure. Total experimental pressures were between 0.67 and 0.69 Pa. DC plasma power was kept at 100 W. Rotation speed for the substrate holder was set to 40 rpm. The argon flow rate Q(Ar) was of 50 sccm, while oxygen flow rate $Q(O_2)$ was changed in a wide range 0.2–0.8 sccm.

The deposited thin films were heat-treated in air at 523 and 623 K for 60 min and cooled to room temperature.

2.2. Characterization

XPS valence-band and core-level spectra were measured using the UHV-Analysis-System (SPECS, Germany) equipped with a PHOIBOS 150 hemispherical energy analyzer. A base pressure was less than $5{\cdot}10^{-10}$ mbar. The XPS spectra were excited by MgK_α source of x-ray radiation ($E = 1253.6$ eV) and were recorded at constant pass energy of 25 eV. The charging effects were taken into account in reference to the C1s line (284.6 eV) of adventitious carbon as it is recommended for such kind of materials [21].

The OK_α-emission bands associated with O2p–O1s transitions and representing the energy distributions of the occupied valence oxygen p-states in the samples were measured by ultra-soft x-ray emission spectroscopy (USXES) using an RSM-500 x-ray monochromator-spectrometer ('Burevestnik', St. Petersburg, Russian Federation). The samples were investigated at an accelerating voltage

$U_a = 5$ kV and an anode current $I_a = 2.5$ mA. Measurements were carried out using a scanning detector based on the secondary electron multiplier KBL1505 (Dr. Sjuts Optotechnik GmbH, Germany). The energy resolution of the RSM-500 was approximately of 0.2 eV. The energy position of the OK_α-emission bands was determined relative to the CrL_λ line.

3. RESULTS AND DISCUSSION

3.1. Oxygen Flow Rate Effect

3.1.1. Analysis of Wide Scan Photoemission Spectra

Wide scan XPS spectra of ITO50 thin films deposited at different oxygen flow rates are presented in Fig. 1, *a*.

All spectra show four major peaks, which correspond to oxygen, tin, indium and carbon presence. C1*s* peak in spectra appeared because of contaminations due to exposure to air.

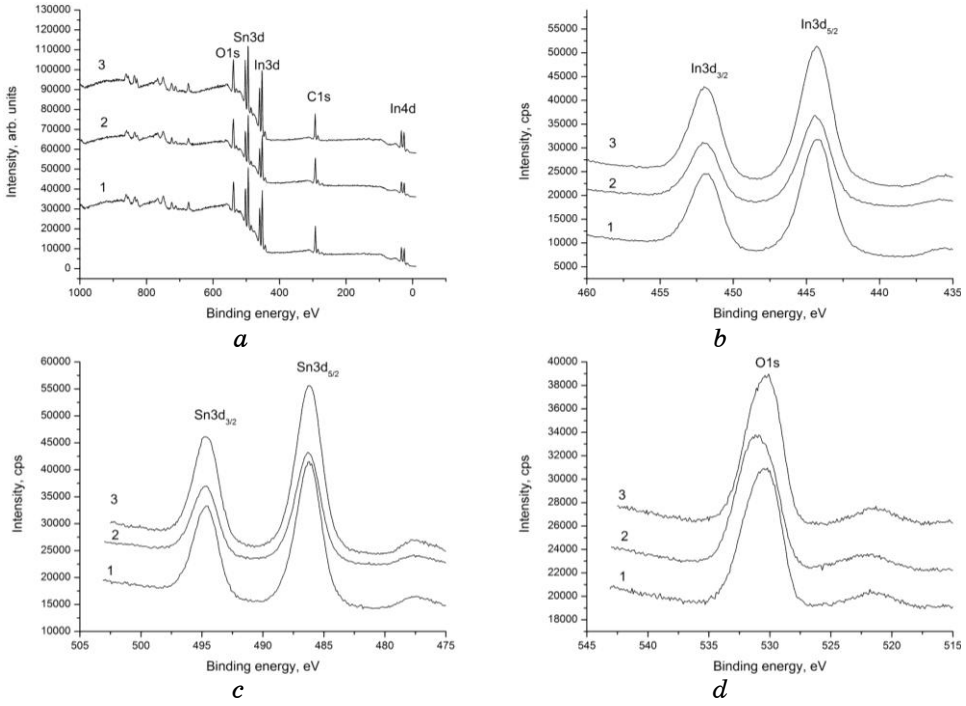

Fig. 1. (*a*) Wide scan XPS spectra, (*b*) In3*d*, (*c*) Sn3*d*, (*d*) O1s XPS spectra of ITO50 thin film sputtered at different oxygen flow rates: *1*—0.3 sccm, *2*—0.5 sccm, *3*—0.8 sccm.

Wide scan XPS spectra of films sputtered at different flow rates are almost similar. The only difference is slight changes in peaks intensities.

3.1.2. Analysis of Core Level Photoemission Spectra

X-ray photoemission spectroscopy (XPS) measurements were carried out in order to find chemical-bonding states of ITO films. The In3*d*, Sn3*d* and O1*s* XPS spectra of the as-deposited ITO50 thin films sputtered at different oxygen flow rates are shown in Fig. 1, *b*–*d*. The shift due to the charging effect was excluded since the C1*s* peak was used as a reference.

According to Fig. 1, *b* and Table 1, the binding energies of $In3d_{3/2}$ and $In3d_{5/2}$ core electrons are of 452.0 ± 0.1 and 444.3 ± 0.1 eV in films sputtered at 0.5–0.8 sccm oxygen flow rate, whereas ITO50 thin film deposited at 0.3 sccm showed slightly lower binding energies. The $In3d_{5/2}$ peak at 444.3 eV corresponds to the In^{3+} charge state. The difference of binding energy of $In3d_{3/2}$ and $In3d_{5/2}$ peaks is of 7.6 ± 0.1 eV, and such a value for $Sn3d_{3/2}$ and $Sn3d_{5/2}$ peaks is of 8.4 ± 0.1 eV, as it was observed for ITO90 thin films by Liu Jing and Zuo Yan [22]. So, chemical states of indium atoms of ITO50 thin films sputtered at different oxygen flow rates are the same. The same tendency was observed for tin atoms.

The binding energies of $Sn3d_{3/2}$ and $Sn3d_{5/2}$ peaks are similar for all deposition conditions, and they are equal to 494.6 and 486.2 eV, respectively. The peak at 486.2 eV is assigned to the binding energy of XPS core-level $Sn3d_{5/2}$ electrons that corresponds to the Sn^{4+} charge state.

So, indium is in one charge state, namely, In^{3+}, and tin exists

TABLE 1. The binding energies of In3*d*, Sn3*d* and O1*s* peaks of ITO50 thin films sputtered at different oxygen flow rates.

Oxygen flow rate, sccm	$In3d_{3/2}$ peak position, eV	$In3d_{5/2}$ peak position, eV	The difference of BE of $In3d_{3/2}$ and $In3d_{5/2}$, eV	$Sn3d_{3/2}$ peak position, eV	$Sn3d_{5/2}$ peak position, eV	The difference of BE of $Sn3d_{3/2}$ and $Sn3d_{5/2}$, eV	O1*s* peak position, eV
0.3	451.8	444.2	7.6 ± 0.1	494.6	486.2	8.4 ± 0.1	530.4
0.5	452.0	444.4	7.6 ± 0.1	494.6	486.2	8.4 ± 0.1	531.1
0.8	452.0	444.4	7.6 ± 0.1	494.6	486.2	8.4 ± 0.1	530.3

only in Sn^{4+} charge state in ITO50 thin films sputtered at different oxygen flow rates.

Figure 1, *d* shows the XPS O1*s* spectra of the as-deposited ITO50 thin films sputtered at different oxygen flow rates. The binding energies of O1s peak are listed in Table 1. O1*s* peak shifts by 0.7 eV towards the higher energies with increasing oxygen flow rate from 0.3 to 0.5 sccm. Full widths at half-maximum of the XPS O1s spectra are similar for thin films sputtered at 0.3 and 0.5 sccm oxygen flow rates, whereas thin film deposited at oxygen flow rate of 0.8 sccm demonstrates decrease of full widths at half-maximum by 0.3 eV (Table 2).

The component ratios of Sn/In and O/(In + Sn) were calculated

TABLE 2. Full width at half-maximum of In3*d*, Sn3*d* and O1*s* peaks for ITO50 thin films sputtered at different oxygen flow rates.

Oxygen flow rate, sccm	Full width half-maximum, eV
$In3d_{5/2}$	
0.3	2.6
0.5	2.4
0.8	2.6
$Sn3d_{5/2}$	
0.3	2.5
0.5	2.4
0.8	2.6
O1*s*	
0.3	3.7
0.5	3.7
0.8	3.4

TABLE 3. Influence of different oxygen flow rates on the atomic concentration in the as-deposited ITO50 thin films.

Oxygen flow rate, sccm	In atomic concentration, %	Sn atomic concentration, %	O atomic concentration, %	O/(In + Sn)	Sn/In	Volume resistivity, μΩ·cm
0.3	20	20	60	1.5	1	1010
0.5	16	17	67	2.03	1.06	694
0.8	23	22	55	1.2	0.96	1420

from the XPS spectra (Table 3).

The present results demonstrate that the film sputtered at oxygen flow rate of 0.5 sccm showed the highest Sn/In value of 1.06. The Sn concentration relative to the In concentration in thin film deposited at oxygen flow rate of 0.5 sccm is higher than in other films, thus, increasing the carrier concentration on the surface of the film [23].

Also, O/(In + Sn) ratio of thin film deposited at oxygen flow rate of 0.5 sccm showed the highest value of 2.03.

The O1*s* spectra can be resolved into three peaks according to Gaussian function, as shown in Fig. 2.

The O1*s* peak consists of three components. The first one O_I at binding energy of 529.2 ± 0.4 eV can be assigned to In ions fully bonded with neighbouring O^{2-} ions; the second one O_{II} at 530.3 ± 0.5 eV is attributed to O–In bonding state in oxygen-deficient region [24]; and the third peak O_{III} at 531.6 ± 0.4 eV is attributed with oxygen-bearing species adsorbed from laboratory air due to its long exposure to ambient conditions prior to the present XPS experi-

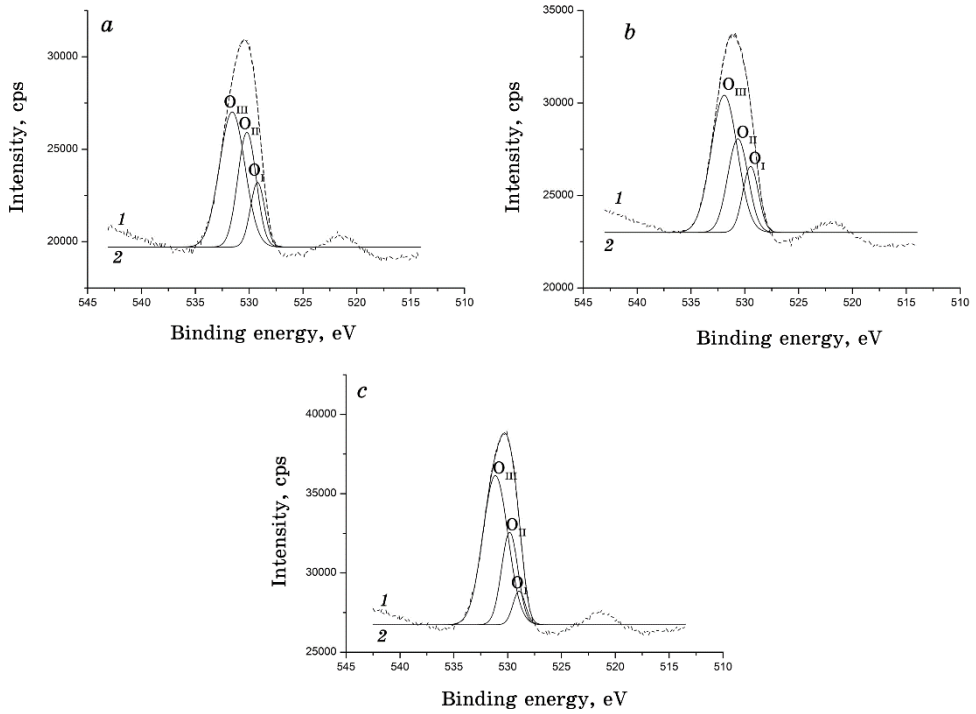

Fig. 2. Deconvolved XPS spectra in the O1*s* region for the ITO50 films sputtered under different oxygen flow rates: (*a*) 0.3 sccm; (*b*) 0.5 sccm; (*c*) 0.8 sccm. *1*—experimental curve; *2*—O_I–O_{III} peaks sum.

ments. O_{II} peak relative intensity increases with increased oxygen vacancies [24].

ITO50 thin film sputtered at 0.5 sccm oxygen flow rate with the highest conductivity demonstrated the highest O_{II} peak relative intensity (Table 4).

3.1.3. Analysis of Valence Band Photoemission Spectra

Low binding energy region in XPS of ITO50 thin films sputtered at different oxygen flow rates containing valence band is presented in Fig. 3.

However, it is difficult to interpret the valence-band spectra, since In4*d* spectra exited by Mg$K_{\alpha 3,4}$ satellites superimpose XPS spectrum of valence electrons in the vicinity of peculiarity *B*.

One can see that the density of states (DOS) of ITO50 thin film decreased, when oxygen flow rate increased from 0.3 sccm to 0.5 sccm. With increasing oxygen flow rate from 0.5 sccm to 0.8 sccm, DOS increased.

TABLE 4. Ratios of the amount of oxygen atoms causing O_I, O_{II}, O_{III} to that of indium atoms in the ITO50 films.

Oxygen flow rate, sccm	O_I/In	O_{II}/In	O_{III}/In	O_{total}/In
0.3	0.14	0.25	0.30	0.46
0.5	0.19	0.27	0.40	0.57
0.8	0.07	0.20	0.32	0.41

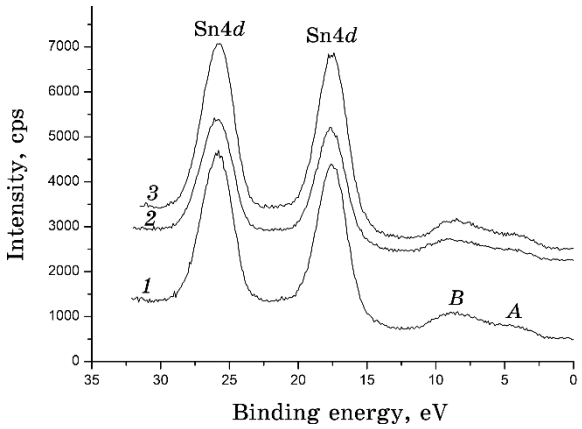

Fig. 3. Low binding energy region in XPS of ITO50 thin films sputtered at different oxygen flow rates containing valence band, In4*d* and Sn4*d* core level structure: *1*—0.3 sccm; *2*—0.5 sccm; *3*—0.8 sccm.

3.2. Heat-Treatment Temperature Effect

Wide scan spectra showing C1*s*, In3*d*, Sn3*d*, O1*s* maxima (Fig. 4, *a*) appear in all films independently on heat-treatment (HT) temperature. However, HT 523 K ITO50 thin film sputtered at 0.5 sccm oxygen flow rate demonstrates the highest peaks' intensity. Core level In3*d* (*a*), Sn3*d* (*b*), and O1*s* (*c*) XPS spectra of the as-deposited and heat-treated at 523 K and 623 K ITO50 thin films sputtered at 0.5 sccm oxygen flow rate are shown in Fig. 4, *b*–*d*. According to Fig. 4, *b*, the binding energies of $In3d_{3/2}$ and $In3d_{5/2}$ peaks are of 452.0 ± 0.1 and 444.3 ± 0.1 eV in as-deposited and heat-treated films. The $In3d_{5/2}$ peak at 444.3 ± 0.1 eV corresponds to the In^{3+} charge state. The binding energies of $Sn3d_{3/2}$ and $Sn3d_{5/2}$ peaks (Fig. 4, *c*) are of 494.6 ± 0.1 and 486.2 ± 0.1 eV, respectively. The peak at 486.2 ± 0.1 eV is assigned to the binding energy of $Sn3d_{5/2}$ peak that corresponds to the Sn^{4+} charge state. Figure 4, *d* shows the XPS O1s spectra of the as-deposited and heat-treated ITO50 thin films.

The binding energies of O1s peak are listed in Table 5. O1*s* peak

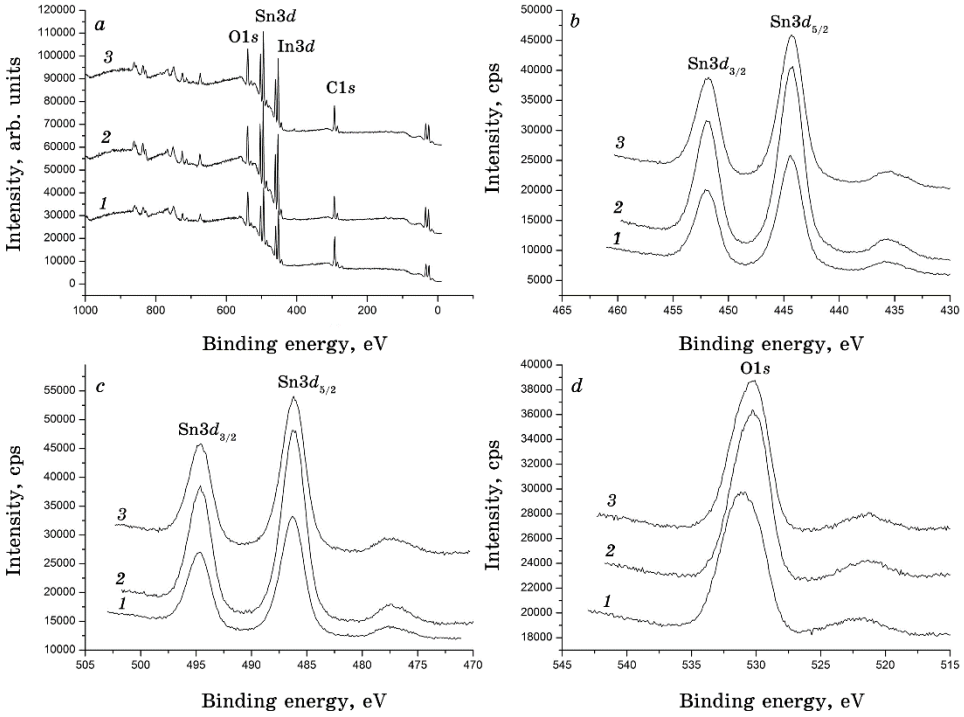

Fig. 4. (*a*) Wide scan XPS spectra, (*b*) In3*d*, (*c*) Sn3*d*, (*d*) O1*s* XPS spectra of the (*1*) as-deposited and (*2*) heat-treated at 523 K and (*3*) at 623 K ITO50 thin film sputtered at 0.5 sccm oxygen flow rate.

TABLE 5. The binding energies of In3*d*, Sn3*d* and O1*s* peaks of ITO50 thin films sputtered at different heat-treatment temperatures at 0.5 sccm oxygen flow rate.

Sample	$In3d_{3/2}$, eV	$In3d_{5/2}$, eV	The difference of BE of $In3d_{3/2}$ and $In3d_{5/2}$, eV	$Sn3d_{3/2}$, eV	$Sn3d_{5/2}$, eV	The difference of BE of $Sn3d_{3/2}$ and $Sn3d_{5/2}$, eV	O1*s*, eV
as-deposited	452	444.4	7.6 ± 0.1	494.8	486.4	8.4 ± 0.1	531.1
HT 523 K	451.9	444.3	7.6 ± 0.1	494.7	486.3	8.4 ± 0.1	530.3
HT 623 K	451.9	444.3	7.6 ± 0.1	494.7	486.3	8.4 ± 0.1	530.3

TABLE 6. Influence of different heat-treatment temperatures on the atomic concentration in the ITO50 thin films sputtered at 0.5 sccm oxygen flow rate.

Sample	In atomic concentration, %	Sn atomic concentration, %	O atomic concentration, %	O/(In + Sn)	Sn/In	Volume resistivity, μΩ·cm
as-deposited	16	17	67	2.03	1.06	694
HT 523 K	18.5	22	59.5	1.46	1.19	683
HT 623 K	21	19	60	1.5	0.9	1220

shifts by 0.8 eV towards the higher energies, when going from as-deposited to heat-treated thin film.

The Sn concentration relative to In concentration (Table 6) in HT 523 K thin film deposited at oxygen flow rate of 0.5 sccm is higher than in other films, thus, increasing the carrier concentration on the surface of the film.

The O1*s* spectra were resolved into three peaks according to Gaussian function, as shown in Fig. 5.

O_{II}/In ratio increased, when going from as-deposited thin film to HT 523 K one, and then decreased (Table 7), whereas volume resistivity decreased, when going from as-deposited thin film to HT 523 K one, and increased for HT 623 K thin film.

Thin film heat-treated at HT 523 K showed the highest O_{II}/In ratio and, therefore, increased amount of oxygen vacancies; so, it has

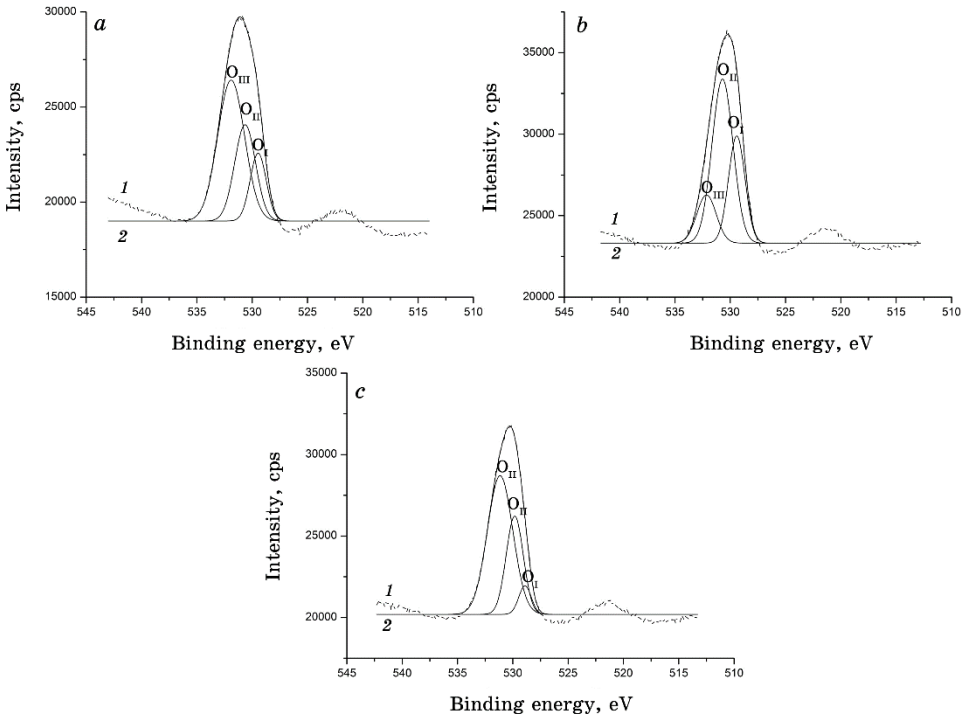

Fig. 5. Deconvolved XPS spectra in the O1*s* region for the as-deposited (*a*) and heat-treated at 523 K (*b*) and at 623 K (*c*) ITO50 films sputtered under 0.5 sccm oxygen flow rate. *1*—experimental curve, *2*—O_I–O_{III} peaks sum.

TABLE 7. Ratios of the amount of oxygen atoms causing O_I, O_{II}, O_{III} to that of indium atoms in the ITO50 films.

Sample	O_I/In	O_{II}/In	O_{III}/In	O_{total}/In	Volume resistivity, μΩ·cm
as-deposited	0.19	0.27	0.40	0.57	694
HT 523 K	0.21	0.33	0.09	0.41	683
HT 623 K	0.07	0.25	0.36	0.49	1220

the lowest volume resistivity.

Intensities of Sn4*d* and In4*d* peaks increased by 1.4 times, when going from as-deposited to HT 523 K thin film, and then decreased in HT 623 K thin films (Fig. 6).

The density of states (DOS) of ITO50 thin film increased, when going from as-deposited to HT 523 K thin film, and then decreased. The highest DOS was shown by ITO50 thin film with the highest conductivity.

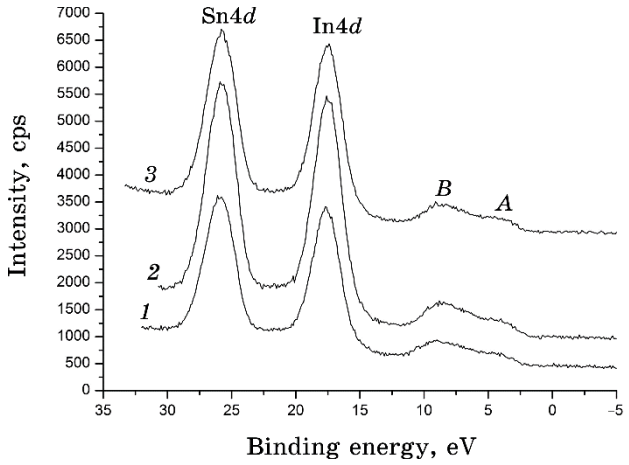

Fig. 6. Low binding energy region in XPS of the (*1*) as-deposited and (*2*) heat-treated at 523 K and (*3*) at 623 K ITO50 thin films sputtered at 0.5 sccm oxygen flow rate.

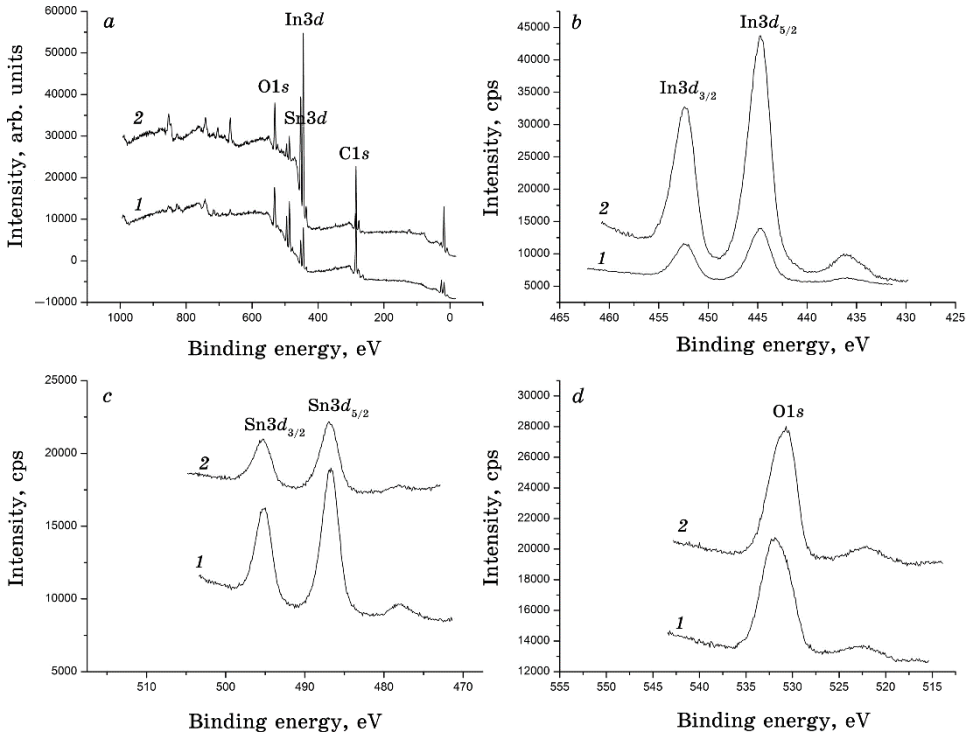

Fig. 7. Wide scan XPS spectra, (*b*) In3*d*, (*c*) Sn3*d*, (*d*) O1*s* XPS spectra of the as-deposited ITO50 (*1*) and ITO90 (*2*) thin films sputtered at 0.2 sccm oxygen flow rate.

3.3. TiN Content Effect

Wide scan spectra showing C1*s*, In3*d*, Sn3*d*, O1*s* maxima (Fig. 7, *a*) appear in both ITO90 and ITO50 thin films.

Core level In3*d* (*a*), Sn3*d* (*b*) and O1*s* (*c*) XPS spectra of the as-deposited ITO90 and ITO50 thin films sputtered at 0.2 sccm oxygen flow rate are shown in Fig. 7, *b*–*d*.

As can be seen from Fig. 7, *b*, the binding energies of $In3d_{3/2}$ and $In3d_{5/2}$ peaks are of 452.4 ± 0.1 and 444.7 ± 0.1 eV in as-deposited ITO90 and ITO50 films. The $In3d_{5/2}$ peak at 444.7 ± 0.1 eV corresponds to the In^{3+} charge state. The binding energies of $Sn3d_{3/2}$ and $Sn3d_{5/2}$ peaks (Fig. 7, *c*) are of 495.2 ± 0.1 and 486.8 ± 0.1 eV, respectively. The peak at 486.8 ± 0.1 eV is assigned to the binding energy of $Sn3d_{5/2}$ peak that corresponds to the Sn^{4+} charge state. Figure 7, *d* shows the XPS O1*s* spectra of the ITO90 and ITO50 thin films. The binding energies of O1s peak are of 531.8 ± 0.1 and 530.7 ± 0.1 eV for ITO50 and ITO90, respectively. O1*s* peak shifts by 1.1 eV towards the higher energies, when going from ITO90 to ITO50. The shift in oxygen O1*s* peak may be due to the increase in oxygen to metal ratio with an increase in the doping concentration [25].

Figure 8 shows valence-band XPS spectra of the as-deposited ITO50 and ITO90 thin films sputtered at 0.2 sccm oxygen flow rate.

The density of states (DOS) of ITO thin film increased, when going from ITO50 to ITO90 thin film. The highest DOS was shown by ITO90 thin film with the highest conductivity.

The OK_α-emission spectra of ITO50 and ITO90 were also recorded and compared on a common energy scale with the XPS valence-band spectra of these films (Fig. 9), following the technique described in detail in [26].

Peculiarity *A* of the XPS valence-band spectra of ITO50 and ITO90 coincides with the maximum of the OK_α-emission spectra of ITO50 and ITO90. Therefore, the sub-band *A* at the top of the valence band of ITO thin films is formed mainly by contributions of O2*p* states.

4. SUMMARY

Indium-saving ITO thin films have been deposited onto glass substrates preheated at 523 K by DC sputtering at different oxygen flow rates and subsequently heat-treated. In order to reduce indium usage in ITO films, an amount of indium oxide in the target was decreased from 90 to 50 mass.%. X-ray photoelectron spectroscopy and x-ray emission spectroscopy were used to reveal effects of oxygen flow rate, Sn content and heat-treatment temperature on elec-

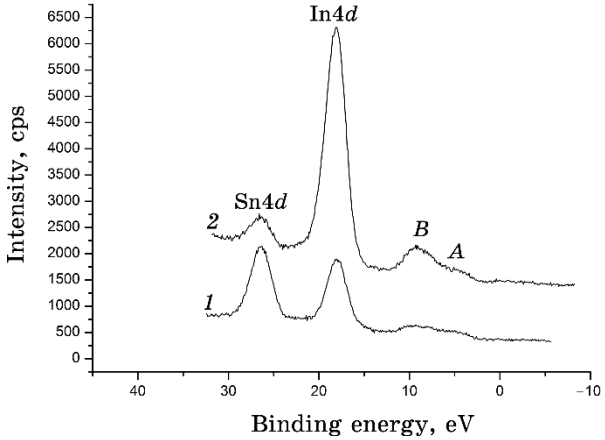

Fig. 8. Low binding energy region in XPS of the as-deposited ITO50 (*1*) and ITO90 (*2*) thin films sputtered at 0.2 sccm oxygen flow rate.

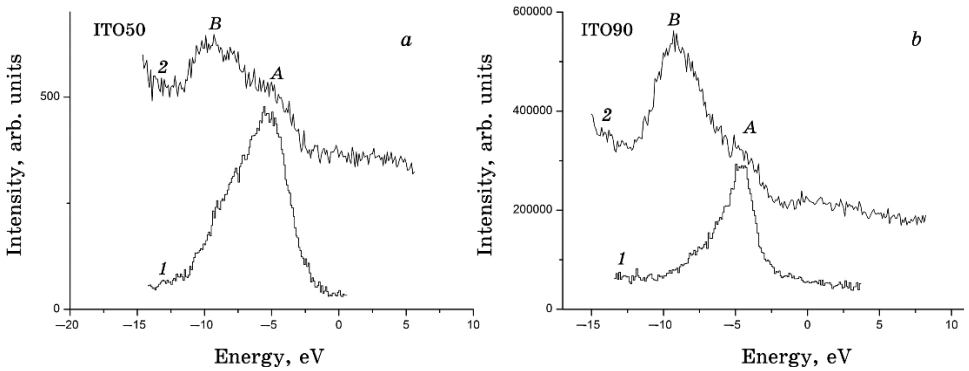

Fig. 9. Valence-band spectra of as-deposited ITO50 (*a*) and ITO90 (*b*) thin films sputtered at 0.2 sccm oxygen flow rate. *1*—USXES; *2*—XPS.

tronic properties.

XPS measurements showed that indium is in one charge state, namely, In^{3+}, and tin exists only in Sn^{4+} charge state in ITO50 thin films sputtered at different oxygen flow rates. Heat treatment does not effect on the charge state of In and Sn. Indium and tin do not change charge state, when going from indium-saving ITO thin films to typical ones. The Sn concentration relative to In concentration in as-deposited thin film sputtered at oxygen flow rate of 0.5 sccm is higher than in other films, thus, increasing the carrier concentration on the surface of the film. As-deposited ITO50 thin film sputtered at 0.5 sccm oxygen flow rate with the highest conductivity demonstrated the highest relative intensity of O_{II} peak, which is at-

tributed to O–In bonding state in oxygen-deficient region.

Thin film deposited at oxygen flow rate of 0.5 sccm and heat-treated at 523 K showed the highest O_{II}/In ratio and, therefore, increased amount of oxygen vacancies. This film demonstrated the lowest volume resistivity.

The density of states increased, when going from ITO50 to ITO90 thin film.

ACKNOWLEDGMENTS

The present research was supported by New Energy and Industrial Technology Development Organization (NEDO), Japan.

REFERENCES

1. S.-Y. Lien, *Thin Solid Films*, **518**: S10 (2010); https://doi.org/10.1016/j.tsf.2010.03.023
2. U. Betz, M. K. Olsson, J. Marthy, M. F. Escolá, and F. Atamny, *Surf. Coat. Technol.*, **200**: 5751 (2006); https://doi.org/10.1016/j.surfcoat.2005.08.144
3. K. P. Sibin, N. Swain, P. Chowdhury, A. Dey, N. Sridhara, H. D. Shashikala, A.K. Sharma, and H. C. Barshilia, *Sol. Energy Mater. Sol. Cells*, **145**: 314 (2016); https://doi.org/10.1016/j.solmat.2015.10.035
4. P. Dai, J. Lu, M. Tan, Q. Wang, Y. Wu, L. Ji, L. Bian, S. Lu, and H. Yang, *Chin. Phys. B*, **26**: 037305 (2017); https://doi.org/10.1088/1674-1056/26/3/037305
5. L. Voisin, M. Ohtsuka, S. Petrovska, R. Sergiienko, and T. Nakamura, *Optik*, **156**: 728 (2018); https://doi.org/10.1016/j.ijleo.2017.12.021
6. P. K. Biswas, A. De, K. Ortner, and S. Korder, *Mater. Lett.*, **58**: 1540 (2004); https://doi.org/10.1016/j.matlet.2003.10.023
7. M. Thirumoorthi and J. Thomas Joseph Prakash, *J. Asian Ceram. Soc.*, **4**: 124 (2016); https://doi.org/10.1016/j.jascer.2015.11.001
8. K. Utsumi, H. Iigusa, R. Tokumaru, P. K. Song, and Y. Shigesato, *Thin Solid Films*, **445**: 229 (2003); https://doi.org/10.1016/S0040-6090(03)01167-2
9. T. Minami, Y. Takeda, S. Takata, and T. Kakumu, *Thin Solid Films*, **308–309**: 13 (1997); https://doi.org/10.1016/S0040-6090(97)00530-0
10. D. H. O'Neil, V. L. Kuznetsov, R. M. J. Jacobs, M. O. Jones, and P. P. Edwards, *Mater. Chem. Phys.*, **123**: 152 (2010); https://doi.org/10.1016/j.matchemphys.2010.03.075
11. S. Li, X. Qiao, and J. Chen, *Mater. Chem. Phys.*, **98**: 144 (2006); https://doi.org/10.1016/j.matchemphys.2005.09.012
12. M. Epifani, R. Diaz, J. Arbiol, P. Siciliano, and J. R. Morante, *Chem. Mater.*, **18**: 840 (2006); https://doi.org/10.1021/cm0522477
13. V. G. Kytin, V. A. Kulbachinskii, O. V. Reukova, Y. M. Galperin, T. H. Johansen, S. Diplas, and A. G. Ulyashin, *Appl. Phys. A*, **114**: 957 (2013); https://doi.org/10.1007/s00339-013-7799-8
14. V. Christou, M. Etchells, O. Renault, P. J. Dobson, O. V. Salata,

G. Beamson, and R. G. Egdell, *J. Appl. Phys.*, **88**: 5180 (2000); https://doi.org/10.1063/1.1312847
15. K. Jung, S. Park, Y. Lee, Y. Youn, H. Shin, H. Kim, H. Lee, and Y. Yi, *Appl. Surf. Sci.*, **387**: 625 (2016); https://doi.org/10.1016/j.apsusc.2016.06.157
16. H. Odaka, Y. Shigesato, T. Murakami, and S. Iwata, *Jpn. J. Appl. Phys.*, **40**: 3231 (2001); https://doi.org/10.1143/JJAP.40.3231
17. A. Chen, K. Zhu, H. Zhong, Q. Shao, and G. Ge, *Sol. Energy Mater. Sol. Cells*, **120**: 157 (2014); https://doi.org/10.1016/j.solmat.2013.08.036
18. D. H. O'Neil, A. Walsh, R. M. J. Jacobs, V. L. Kuznetsov, R. G. Egdell, and P. P. Edwards, *Phys. Rev. B*, **81**: 085110 (2010); https://doi.org/10.1103/PhysRevB.81.085110
19. C.-Y. Ren, S.-H.Chiou, and J. Choisnet, *J. Appl. Phys.*, **99**: 023706 (2006); https://doi.org/10.1063/1.2163017
20. D. H. O'Neil, R. G. Egdell, and P. P. Edwards, *J. Appl. Phys.*, **107**: 093702 (2010); https://doi.org/10.1063/1.3399769
21. W.-F. Wu and B.-S. Chiou, *Semicond. Sci. Technol.*, **11**: 196 (1996); https://doi.org/10.1088/0268-1242/11/2/009
22. L. Jing and Z. Yan, *J. Wuhan Univ. Technol.-Mater. Sci. Ed.*, **25**: 753 (2010); https://doi.org/10.1007/s11595-010-0086-z
23. J. S. An, S. C. Kim, S. H. Hahn, S. K. Ko, *J. Korean Phys. Soc.*, **45**: 1629 (2004); https://www.jkps.or.kr/journal/view.html?uid=6518&vmd=Full
24. J. C. C. Fan and J. B. Goodenough, *J. Appl. Phys.*, **48**: 3524 (1977); https://doi.org/10.1063/1.324149
25. S. V. Pammi, A. Chanda, J.-K. Ahn, Jo.-H. Park, C.-R. Cho, W.-J. Lee, and S.-G. Yoon, *J. Electrochem. Soc.*, **157**: H937 (2010); https://doi.org/10.1149/1.3467802
26. O. Y. Khyzhun, Y. V. Zaulychny, and E. A. Zhurakovsky, *J. Alloys Compd.*, **244**: 107 (1996); https://doi.org/10.1016/S0925-8388(96)02412-7